

PAPER • OPEN ACCESS

## Impact of inversion symmetry on a quasi-1D $S = 1$ system

To cite this article: J K Kim *et al* 2020 *J. Phys.: Condens. Matter* **32** 225802

View the [article online](#) for updates and enhancements.



**IOP | ebooks™**

Bringing together innovative digital publishing with leading authors from the global scientific community.

Start exploring the collection—download the first chapter of every title for free.

# Impact of inversion symmetry on a quasi-1D $S = 1$ system

J K Kim<sup>1,2</sup>, K M Ranjith<sup>1</sup> , U Burkhardt<sup>1</sup>, Yu Prots<sup>1</sup>, M Baenitz<sup>1</sup>  
and M Valldor<sup>1,3</sup> 

<sup>1</sup> Max Planck Institute for Chemical Physics of Solids, Nöthnitzer Str. 40, 01187 Dresden, Germany

<sup>2</sup> Department of Physics, Pohang University of Science and Technology, Pohang 790-784, Republic of Korea

<sup>3</sup> Department of Chemistry, Centre for Materials Science and Nanotechnology (SMN), University of Oslo, PO Box 1033 Blindern, N-0315 Oslo, Norway

E-mail: [b.m.valldor@kjemi.uio.no](mailto:b.m.valldor@kjemi.uio.no)

Received 20 November 2019, revised 17 January 2020

Accepted for publication 29 January 2020

Published 3 March 2020



## Abstract

Here, we report the synthesis and magnetic properties of a novel, centrosymmetric, quasi-1D spin chain system  $\text{La}_3\text{VWS}_3\text{O}_6$ , with hexagonal crystal structure ( $P6_3/m$ ,  $a = 9.46076(3)$ ,  $c = 5.51809(2)$  Å). Pure powders were obtained by solid-state reactions from  $\text{La}_2\text{O}_3$ ,  $\text{WO}_3$  and metal powders of V and W. X-ray powder diffraction, specific heat, magnetization,  $^{139}\text{La}$ -nuclear magnetic resonance (NMR), and electric resistivity measurements indicate that the compound is a low dimensional magnet with an  $S = 1$  spin chain that exhibits no sign of magnetic ordering above 2 K. A single ion anisotropy ( $D/k_B \sim 10$  K), caused by magneto-crystalline effects, is probably responsible for a thermodynamic entropy release at lower temperatures, which concurs with  $^{139}\text{La}$ -NMR data. By detailed comparison with non-centrosymmetric  $\text{Ba}_3\text{V}_2\text{S}_4\text{O}_3$ , having a very similar magnetic lattice, it is obvious that the presence of crystallographic inversion symmetry has an effect on the behaviour of the magnetic chains.

Keywords: low-dimensional magnetism,  $S = 1$ , inversion symmetry, magneto-electric coupling


(Some figures may appear in colour only in the online journal)

## 1. Introduction

Quasi-one-dimensional (1D) magnetic systems exhibit complex excitation spectra, which are far from being completely understood [1]. Moreover, 1D materials always were an active research topic because of their unique properties and potential electrical applications [2–4]. In theoretical investigations, 1D chains with non-classical spin, such as  $S = 1/2$  and  $S = 1$ , have gained considerable attention due to their relatively simple descriptions. For instance, 1D system containing  $S = 1/2$  chains without spin-excitations (gapless) are often referred to as Luttinger liquids, featuring a spin-charge separation [5, 6].

In contrast, 1D  $S = 1$  system have a spin excitation gap and belong to the Haldane physics [7, 8].

The understanding and the interest of crystallographic symmetry on magnetic properties was greatly improved by recent works on multiferroics [9, 10] and skyrmion-related spintronics [11], but those magnetic systems are usually quasi 2D or 3D. However, due to lack of physical examples, it has not been thoroughly investigated how the crystallographic inversion symmetry ( $\bar{1}$ ) affects a 1D magnetic lattice. Locally, the absence of inversion symmetry allows for higher-order effects, like Dzyaloshinsky–Moriya interactions (DMI) [12, 13], which describe the spontaneous couplings of magnetic spins to the electronic polarity of the host lattice. These magneto-electric couplings might result in canting of spins, where exotic spin configurations, like spin-spirals in  $\text{Ba}_2\text{CuGe}_2\text{O}_7$  [14], spin cycloids in  $\text{Mn}_{0.95}\text{Co}_{0.05}\text{WO}_4$  [15], or helimagnetism in  $\text{Rb}_2\text{Cu}_2\text{Mo}_3\text{O}_{12}$  [16], are observed. In contrast, a

 Original content from this work may be used under the terms of the [Creative Commons Attribution 4.0 licence](https://creativecommons.org/licenses/by/4.0/). Any further distribution of this work must maintain attribution to the author(s) and the title of the work, journal citation and DOI.

centrosymmetric 1D  $S = \frac{1}{2}$  lattice might involve spin-Peierls transition [17], where two spins dimerize into a singlet states. Consequently, a dimerized  $S = \frac{1}{2}$  antiferromagnetic chain has a well-defined excitation gap [18, 19].

Recently, Bryhan *et al* reported novel 1D bichalcogenides  $\text{La}_3\text{TMWS}_3\text{O}_6$  ( $\text{TM} = \text{Cr, Mn, Fe, Co, Ni}$ ) with centrosymmetric crystal structures [20], but questions remained open concerning their physical properties. Some of those materials could be prepared as pure powders and a first insight in these 1D classical spin magnets was made [21], stating that they exhibit typical low-dimensional magnetism with strong antiferromagnetic spin–spin interactions but without long range spin orderings. The polar, non-centrosymmetric 1D  $S = 1$  compound  $\text{Ba}_3\text{V}_2\text{S}_4\text{O}_3$ , was reported some time ago [22], but was only recently prepared as pure powder [23]: its 1D magnetic lattice does not order above 2K although magnetic anomalies are observed at temperatures up to 140K. For a better comparison, here the novel, centrosymmetric  $\text{La}_3\text{VWS}_3\text{O}_6$  is presented and its properties can be directly compared with those of  $\text{Ba}_3\text{V}_2\text{S}_4\text{O}_3$ , because of the same magnetic ion ( $\text{V}^{3+}$ ,  $S = 1$ ) on a 1D magnetic lattice in both compounds. In the latter the charge disproportionation  $\text{V}^{3+}/\text{V}^{5+}$  was experimentally proven by x-ray spectroscopy [23].

Using the Niggli notation (from here on),  $\text{La}_3\text{VWS}_3\text{O}_6$  and  $\text{Ba}_3\text{V}_2\text{S}_4\text{O}_3$ , with very similar crystal structures, can be rewritten as  $\text{La}_3[\text{WO}_6]_{\infty}^1[\text{VS}_{6/2}]$  and  $\text{Ba}_3[\text{VSO}_3]_{\infty}^1[\text{VS}_{6/2}]$ , respectively, emphasizing the shared feature of the infinite 1D magnetic chain-lattice of face-sharing  $[\text{VS}_{6/2}]$  octahedra. Hence, these two systems have the same magnetic chain lattice, giving an opportunity to probe the effects of the crystallographic inversion symmetry on a 1D  $S = 1$  magnet.

## 2. Materials and methods

### 2.1. Synthesis

A polycrystalline sample of  $\text{La}_3[\text{WO}_6]_{\infty}^1[\text{VS}_{6/2}]$  was prepared by a conventional solid-state reaction technique using  $\text{La}_2\text{O}_3$  (99.99%, Alfa Aesar), V (99.5%, Alfa Aesar), W (99.9%, Alfa Aesar),  $\text{WO}_3$  (99.8%, Alfa Aesar), and S (99.5%, Alfa Aesar) as starting materials. The constituents were homogenized in an agate mortar and pressed into pellets under inert conditions inside an argon glovebox (MBraun Labmaster DP). These pellets were put into a corundum crucible within a silica tube. Subsequently, the silica tube was sealed having an internal pressure of 200mbar of argon. The sample was heated to 1150 °C and held at this temperature for 55h. The pellets became a powder and were reground to ensure good homogeneity. In powder form the sample was re-reacted twice at the same temperature but for 10h with intermediate grindings. Small crystals of  $\text{La}_3[\text{WO}_6]_{\infty}^1[\text{VS}_{6/2}]$  were grown in a KCl melt using  $\text{La}_2\text{O}_3$ , V, W,  $\text{WO}_3$  and S as starting materials. The reagents were funnelled into a silica tube directly, heated to 950 °C, and maintained for 50h. Subsequently, the mixture was cooled down to 500 °C during 50h and allowed to cool to the room temperature at an ambient rate.

### 2.2. Electron microscopy

Energy dispersive x-ray analysis was performed on small crystals of  $\text{La}_3[\text{WO}_6]_{\infty}^1[\text{VS}_{6/2}]$  by Quantax EDX-System (Bruker); Silicon Drift Detector (SDD, 6l30) with Espirit-Software Vers.1.9 inside a scanning electron microscope (SEM) JSM 7800 F (JEOL) equipped with a field emission cathode.

### 2.3. X-ray diffraction

On the same sample that was used for property investigations, x-ray diffraction was measured with  $\text{CuK}\alpha_1$  radiation ( $\lambda = 1.540598 \text{ \AA}$ , Huber camera) and with synchrotron powder x-ray diffraction ( $\lambda = 0.40003 \text{ \AA}$ ) at beamline ID22, ESRF, Grenoble.

### 2.4. Magnetic investigations

For magnetic measurements, powder of  $\text{La}_3[\text{WO}_6]_{\infty}^1[\text{VS}_{6/2}]$  was placed in an airtight polycarbonate capsule (2–350K) or in a silica tube with corundum wool for higher temperatures. The magnetic data were collected by a SQUID magnetometer: Magnetic Property Measurement System (MPMS-XL) from Quantum Design (San Diego). The zero field cooling (ZFC) data were acquired after cooling the sample from 300K to 1.8K without and external field and measuring on heating. The field cooled (FC) data were subsequently obtained on cooling, keeping the same static field.

### 2.5. Specific heat investigation

Specific heat measurements were performed by using a commercial physical property measurement system (PPMS; Quantum Design) by means of standard non-adiabatic thermal relaxation method on the commercial Quantum Design sample holder. The sample consisted of a thin plate of pressed, sintered polycrystalline material (about 5 mg) that was attached to the sample holder using Apiezon grease. At each temperature, the sample was measured twice to rule out temperature drifts and non-equilibrium states and each heat pulse was set to be 2% of the system temperature.

### 2.6. Electrical resistivity

The temperature dependent resistivity was also measured with PPMS from 130K to 300K by a standard four probe method, using silver-glyce and gold wires, on a sintered polycrystalline piece.

### 2.7. Nuclear magnetic resonance

Solid-state nuclear magnetic resonance (NMR) measurements were carried out using a pulsing technique on  $^{139}\text{La}$  nuclei in the temperature range 5–100K using a  $^4\text{He}$  cryostat.  $^{139}\text{La}$  has nuclear spin  $I = 7/2$  and gyromagnetic ratio

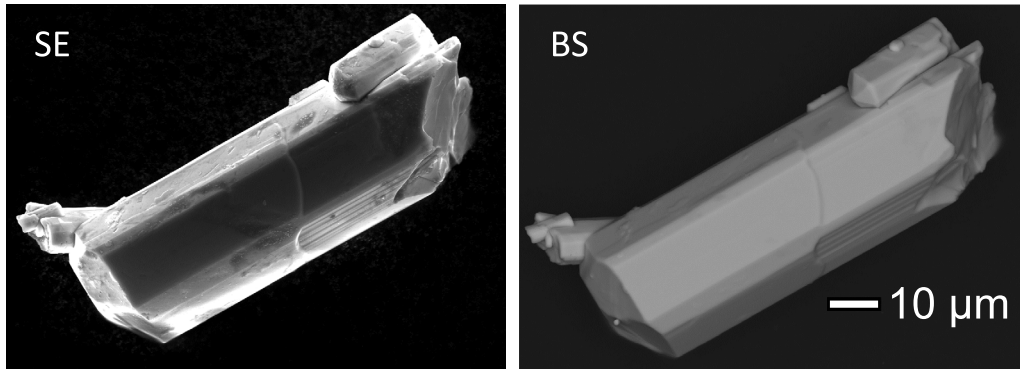


**Figure 1.** SEM images of an agglomeration of several  $\text{La}_3[\text{WO}_6]_\infty[\text{VS}_{6/2}]$  crystals, using either a secondary electron (SE) or a back-scattering (BS) detector. The largest crystal rod is about  $100 \mu\text{m}$  long and exhibits the intimate inter-growth of crystallites.

$\gamma/2\pi = 6.014 \text{ MHz T}^{-1}$ . Field sweep NMR spectra were obtained by plotting the echo integral intensity, i.e. following a  $\pi/2 - \pi$  pulse sequence, as function of field at a fixed frequency of 43.9 MHz. The NMR Knight shifts,  $K = (H_L - H^*)(T)/H^*(T)$ , were estimated by measuring the resonance field  $\mu_0^*H(T)$  of the sample in comparison with the Lamor field ( $H_L$ ) of a non-magnetic La-containing reference compound.

### 3. Results

#### 3.1. Electron microscopy

After the final heat treatment, homogeneous and fine black powders resulted, suggesting that the title compound is a small-gap insulator. EDX analyses on single crystals and powder crystallite suggest the composition  $\text{La}_{3.0(2)}\text{V}_{0.93(3)}\text{W}_{1.0(1)}\text{S}_{3.23(7)}\text{O}_{6.5(3)}$ , as normalized to La. The obtained composition is close to nominal one and, further, no other elements were detected. Figure 1 displays single crystals of  $\text{La}_3[\text{WO}_6]_\infty[\text{VS}_{6/2}]$ , as observed in SEM. The low contrasts in the back-scattering (BS) image suggest that the material is compositionally homogeneous. The single crystal size ranged from 30 to  $100 \mu\text{m}$ , but due to intimate growths, a single domain crystal of usable size, large enough for macroscopic measurements, could not be separated from the salt melts. Single crystal x-ray diffraction data were severely affected by scattering from twin domains. All crystal rods have hexagonal-like habit.

#### 3.2. Crystallography

The crystal structure of  $\text{La}_3[\text{WO}_6]_\infty[\text{VS}_{6/2}]$  was determined by comparing a Rietveld simulation with synchrotron powder x-ray diffraction pattern, and a good agreement was obtained even at high angles as seen in the inset of figure 2. The powder sample is almost pure; the only observed secondary phase was  $\text{WS}_2$  [24] and its relative volume was refined to 1.6 vol% by Rietveld simulation. As this impurity is nonmagnetic and contains no La, it will not significant effect on any of the performed measurements below. All measurement related and crystallographic data from the Rietveld refinement are given in table 1. Data from single crystal diffraction (not listed)

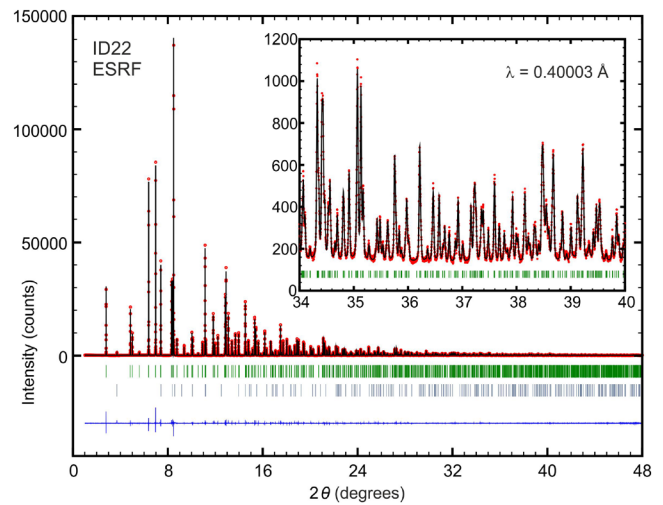


**Figure 2.** Rietveld refinement of synchrotron powder x-ray diffraction pattern of  $\text{La}_3[\text{WO}_6]_\infty[\text{VS}_{6/2}]$  with observations (red dots), calculations (black line), and their differences (blue). Bragg reflections are indicated by vertical lines for the main phase (up) as well as impurity  $\text{WS}_2$  (down). The inset graph shows a magnified part of the high angle data.

agree well with the Rietveld model.  $\text{La}_3[\text{WO}_6]_\infty[\text{VS}_{6/2}]$  is isostructural to  $\text{La}_3[\text{WO}_6]_\infty[\text{TMS}_{6/2}]$  ( $\text{TM} = \text{Cr, Mn, Fe, Co, Ni}$ ) [20]. The  $\text{La}_3[\text{WO}_6]_\infty[\text{VS}_{6/2}]$  structure can be described as a hexagonal packing of chains that consist of face-sharing  $\text{VS}_6$  octahedra and extend along the unique ( $c$ ) axis. Between the chains reside  $\text{WO}_6$  trigonal prisms with the tungsten ions at their centres (figure 3). The lanthanum ions are filling the voids between these two structural motifs. La atoms are located  $4.13 \text{ \AA}$  apart in the apexes of regular triangles, which alternates with  $\text{WO}_6$  prisms along  $[001]$ . For a more complete structural description, see the work of Bryhan *et al* [20].

#### 3.3. Magnetometry

The magnetic susceptibilities,  $\chi(T)$ , of  $\text{La}_3[\text{WO}_6]_\infty[\text{VS}_{6/2}]$ , measured as functions of temperature and at different applied fields, are shown in figure 4.  $\chi(T)$  increases with decreasing temperature and the high temperature data can be fitted with a Curie–Weiss approximation:  $\chi(T) = \chi_0 + \frac{C}{T - \theta_{\text{CW}}}$ , where



**Table 1.** Crystallographic data for the measurement of  $\text{La}_3[\text{WO}_6]_{\infty}^1[\text{VS}_{6/2}]$  and the resulting parameters, as obtained from the Rietveld refinement of synchrotron x-ray powder diffraction data.

Formula		$\text{La}_3\text{VWS}_3\text{O}_6$			
Formula weight ( $\text{g mol}^{-1}$ )		843.7			
Z		2			
Crystal system		Hexagonal			
Space Group		$P6_3/m$ (No. 176)			
$a$ ( $\text{\AA}$ )		9.46076(3)			
$c$ ( $\text{\AA}$ )		5.51809(2)			
Cell volume ( $\text{\AA}^3$ )		427.732(3)			
Calc. density, $\rho$ ( $\text{g cm}^{-3}$ )		6.6			
X-ray radiation source		Synchrotron			
Wavelength ( $\text{\AA}$ )		0.40003(1)			
$2\theta$ range ( $^\circ$ )		1–48			
Abs. coeff.		3.22			
Total reflections		1339			
Total refined parameters		45			
$R(\text{obs})$ , $wR(\text{obs})$		0.017, 0.020			
$R(\text{all})$ , $wR(\text{all})$		0.017, 0.020			
GoF		1.79			
Max peak/hole (elec. $\text{\AA}^{-3}$ )		+2.2/−4.7			
Atom	Wyckoff	$x$	$y$	$z$	$U_{\text{iso}}$
La	$6h$	0.3169(2)	0.4067(2)	$\frac{1}{4}$	0.0046(2)
V	$2b$	0	0	0	0.0046(1)
W	$2d$	$\frac{2}{3}$	$\frac{1}{3}$	$\frac{1}{4}$	0.0023(3)
S	$6h$	0.2283(6)	0.0450(7)	$\frac{1}{4}$	0.006(1)
O	$12i$	0.636(1)	0.1633(9)	0.026(2)	0.005(1)

$\chi_0$  is the temperature independent contribution consisting of core diamagnetism and van-Vleck paramagnetism,  $C$  is the Curie constant and  $\theta_{\text{CW}}$  the Curie–Weiss temperature. In the temperature range 300–700 K (inset figure 4), the fit yields  $C = 1.15(1) \text{ cm}^3 \text{ mol}^{-1} \text{ K}^{-1}$ , and  $\theta_{\text{CW}} = -569(9) \text{ K}$ . The core diamagnetism of involved ions was taken from literature [25],  $\chi_0 = -1.26 \times 10^{-4} \text{ cm}^3 \text{ mol}^{-1}$ .

From the value of  $C$ , the effective moment was calculated to be  $\mu_{\text{eff}} \approx 3.0 \mu_{\text{B}}$ , which is in close agreement with the expected spin-only value of  $2.83 \mu_{\text{B}}$  for  $S = 1$ , assuming the Landé factor ( $g$ ) to be 2. The negative value of  $\theta_{\text{CW}}$  indicates that the dominant exchange couplings between  $\text{V}^{3+}$  ions are antiferromagnetic in nature and that true paramagnetic behaviour will only be observed above 570 K, of which the latter explains the minor deviation from expectancy concerning the estimated magnetic moment ( $\mu_{\text{eff}}$ ). Note, the Curie–Weiss constant suggests that the average antiferromagnetic interaction is relatively strong. However, for every two intra-chain interactions there are six inter-chain interactions, and, if the latter is antiferromagnetic, a geometric frustration results due to the crystallographic hexagonal symmetry. Hence, the antiferromagnetic interactions between the spin-chains might increase the Curie–Weiss temperature but not the size of the spin–spin interaction in each spin-chain.

In figure 4, the  $\chi(T)$  curve at  $\mu_0 H = 1 \text{ T}$  increases as the temperature approaches 2 K. This can be explained by a minor paramagnetic extrinsic signal, probably from an impurity. Upon saturating the Curie–Weiss tail at larger fields, a maximum in the  $\chi(T)$  curve at about 10 K becomes evident that

originates from an intrinsic effect. This maximum agrees well with the release of magnetic entropy (see figure 5).

### 3.4. Heat capacity

As seen in the specific heat measurements (figure 5), a Debye like phonon contribution describes most of the data, that start to saturate close to the expected Dulong–Petit limit:  $3RN = 349.2 \text{ J mol}^{-1} \text{ K}^{-1}$ , where  $R$  is the gas constant and  $N$  is the number of atoms in the chemical formula. Only at low temperatures is it possible to discern a deviation from pure phonon behaviour (upper inset in figure 5); the shown Debye-curve contains high-temperature (30–300 K) measurements of the non-magnetic reference compound  $\text{La}_3[\text{WO}_6]_{\infty}^1[\text{CoS}_{6/2}]$ , where Co is in a low-spin  $d^6$  state [21]. Below 30 K, the Debye-curve was extrapolated down to the ground state with a pure phonon contribution. The low temperature entropy release of  $\text{La}_3[\text{WO}_6]_{\infty}^1[\text{VS}_{6/2}]$  coincides well with the magnetic anomaly (figure 4); a simple integration of the presumed magnetic contribution sums up to the entropy release that is expected for a long range spin order or an  $S = 1$  system:  $R \ln(2S + 1)$ . The entropy is, however, released over a very large temperature, which is not typical for a magnetic spin ordering.

### 3.5. Electrical resistivity

$\text{La}_3[\text{WO}_6]_{\infty}^1[\text{VS}_{6/2}]$  is obviously an insulator with a relatively low conduction activation energy. The electrical resistivity

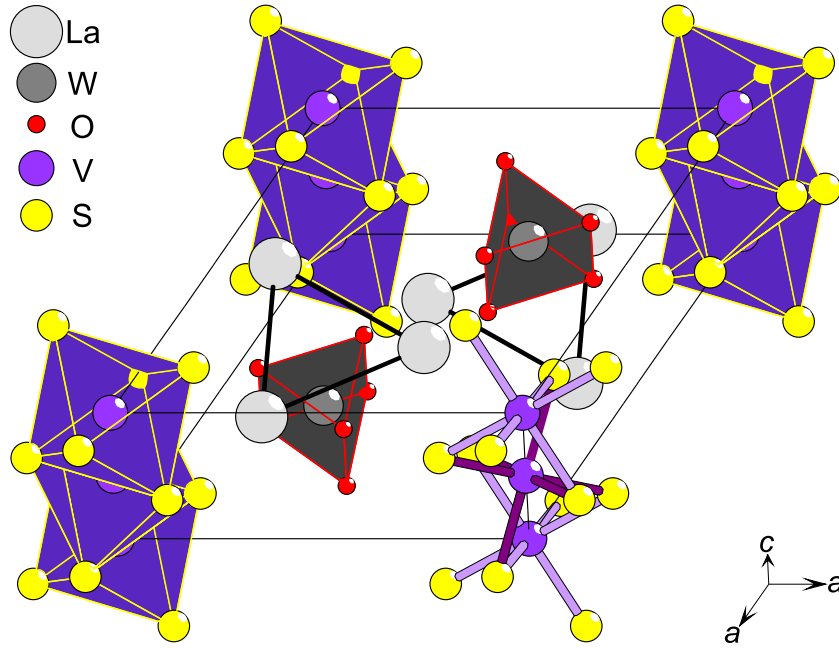


**Figure 3.** Top view of the  $\text{La}_3[\text{WO}_6]_\infty[\text{VS}_{6/2}]$  crystal structure, where the unit cell is marked with thin lines, the  $\text{VS}_6$  octahedra and  $\text{WO}_6$  trigonal prisms are emphasized as polyhedra or with coordination bonds. Thicker lines connect La atoms to clarify that they are situated as trimers.

(data not shown) increases from  $\sim 3 \Omega\text{m}$  at room-temperature up to  $\sim 5 \text{ k}\Omega\text{m}$  at 125 K and a straight forwards Arrhenius estimation of the thermal activation energy delivers a value of  $E_g = 0.12 \text{ eV}$ , according to:  $\sigma = \sigma_0 \times e^{-E_g/2k_B T}$ , where  $\sigma$  is the conductivity,  $E_g$  the activation energy,  $k_B$  the Boltzmann constant. However, the real value might be significantly larger, because the conductivity is affected by crystal imperfections in the bulk and, especially, at grain boundaries.

### 3.6. NMR measurements

The advantage of NMR is that it is a local probe and not sensitive to impurities. Therefore, one can probe the intrinsic properties of the spin system.  $^{139}\text{La}$  NMR field sweep spectra of the central transition (CT:  $-\frac{1}{2}$  to  $+\frac{1}{2}$ ) measured at different temperatures are depicted in figure 6. For a quadrupole nuclei, the nuclear spin Hamiltonian can be expressed as  $\mathcal{H} = -\gamma\hbar\hat{I}_z H (1 + K) + \frac{h\nu_Q}{6} [(3\hat{I}_z^2 - \hat{I}^2) + \eta(\hat{I}_x^2 - \hat{I}_y^2)]$ , where the first term represents the Zeeman interaction and the second term represents the quadrupolar interactions. Here,  $\gamma$  is the gyromagnetic ratio for the nuclei,  $\hbar$  is the Planck's constant,  $H$  is the applied field along  $\hat{z}$ ,  $K$  is the magnetic shift due to hyperfine field at the nuclear site,  $\eta$  is the asymmetry parameter,  $\nu_Q = \frac{3eQV_{ZZ}}{2\hbar(2I-1)}$  is the quadrupole coupling constant,  $V_{ZZ}$  is the largest component of electric field gradient (EFG) tensor, and  $eQ$  is the nuclear quadrupole moment. In polycrystalline samples, each crystallite is arbitrary oriented to the external magnetic field, which yield a distribution of Euler angles and thus a broad powder pattern of NMR spectra. The shape of the powder NMR pattern can be calculated by summing up the all contributions from the possible orientations. The Knight shift measured along the  $z$  direction of the applied magnetic field can be explained as

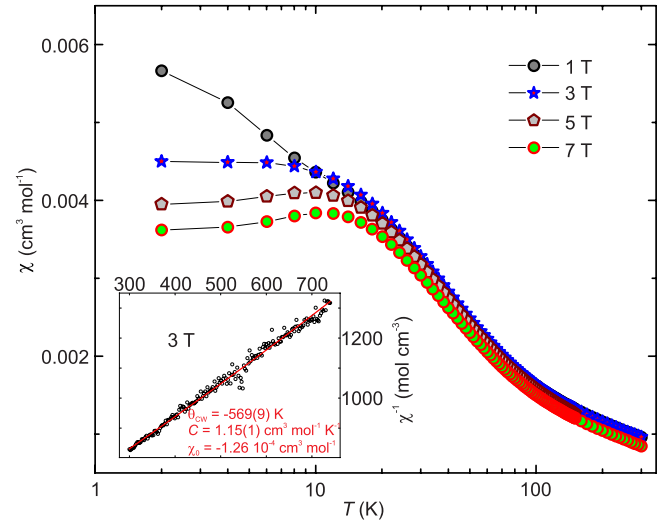


**Figure 4.** Magnetic susceptibilities of polycrystalline  $\text{La}_3[\text{WO}_6]_\infty[\text{VS}_{6/2}]$  as a function of temperature at different applied fields. Inset shows  $\chi^{-1}(T)$  and the solid line is an estimation of the Curie–Weiss law.

$$K_z(\theta, \phi) = K_{X'} \sin^2 \theta \cos^2 \phi + K_{Y'} \sin^2 \theta \sin^2 \phi + K_{Z'} \cos^2 \theta,$$

where  $\theta$  and  $\phi$  be the angles describing the relative orientation of  $(X', Y', Z')$  versus the direction of external magnetic field along  $z$ . Then the anisotropic Knight shifts are obtained as

$$K_{\text{iso}} = \frac{1}{3} (K_{X'} + K_{Y'} + K_{Z'}); K_{\text{aniso}} = \frac{1}{2} (K_{Y'} - K_{X'})$$

$$\text{and } K_{\text{ax}} = \frac{1}{6} (2K_{Z'} - K_{Y'} - K_{X'}).$$

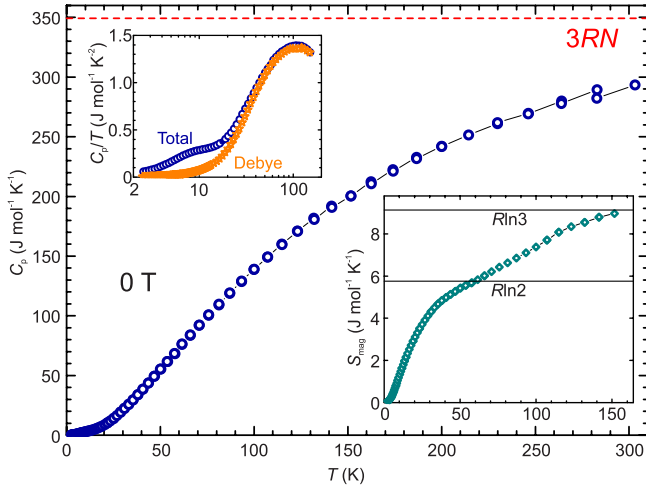


**Figure 5.** Temperature dependence of specific heat of polycrystalline  $\text{La}_3[\text{WO}_6]_\infty[\text{VS}_{6/2}]$  measured at zero magnetic fields, where the Dulong–Petit limit is represented with a dashed line. The upper inset shows a Debye-like contribution as compared with the measured  $C_p/T(T)$  data (Total). The lower inset displays the integrated difference between measured (Total) and phonon (Debye) specific heat signals, where two theoretical entropy levels are marked.

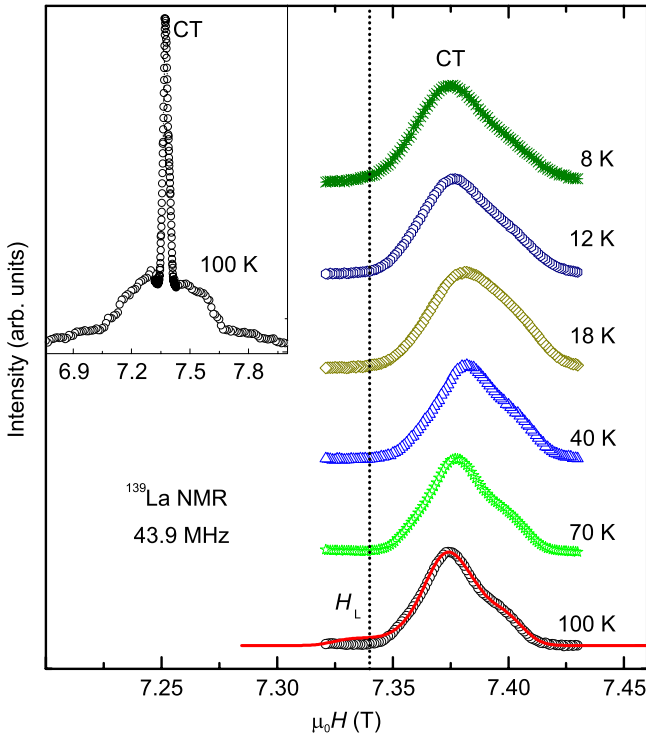


**Figure 6.** Temperature-dependent CT-field-sweep  $^{139}\text{La}$  NMR spectra of polycrystalline  $\text{La}_3[\text{WO}_6]_\infty[\text{VS}_{6/2}]$  measured at 43.9 MHz. The vertical dotted line corresponds to the  $^{139}\text{La}$   $K = 0$  position (Larmor field). The solid red line is the simulation of the spectrum at  $T = 100\text{ K}$  with the parameters given in the text. The inset shows the field L-NMR powder spectra with the narrow central transition (CT).

The 100 K La-NMR spectrum can be fitted well with the parameters  $K_{\text{iso}} \approx -0.505\%$ ,  $K_{\text{ax}} \approx 0.08\%$ ,  $K_{\text{aniso}} \approx -0.09\%$ ,  $\eta = 0$ ,  $\nu_Q \approx 0.24\text{ MHz}$ , and a linewidth  $\approx 59.35\text{ MHz}$ . The

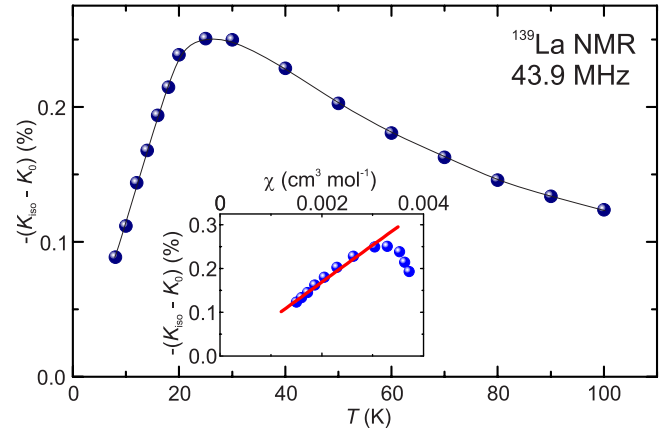


**Figure 7.** Temperature-dependent  $^{139}\text{La}$  NMR shift  $K$  as a function of temperature. Inset:  $K$  versus  $\chi$  measured at 7 T is plotted with temperature as an implicit parameter. The solid (red) line in the inset is the linear fit.

line shape was found to be asymmetric agreeing with the expected anisotropy in  $\chi(T)$  and/or in the hyperfine coupling constant between the La nucleus and the  $\text{V}^{3+}$  spins.

The spectral position was found to shift with temperature and the NMR shift  $K_{\text{iso}}$  dependence could be extracted by fitting the spectra (see figure 6) as presented in figure 7. The NMR shift increases with decreases in temperatures and then passes through a broad maximum at around 20 K again confirming the low-dimensional short-range nature of the magnetic exchange. The NMR shift,  $K(T)$ , is a direct measure of intrinsic spin susceptibility,  $\chi_{\text{spin}}$ , according to:

$$K(T) = K_0 + \frac{A_{\text{hf}}}{N_A} \chi_{\text{spin}}(T),$$

where  $K_0$  is the temperature independent chemical shift,  $A_{\text{hf}}$  is the transferred hyperfine coupling constant between the  $^{139}\text{La}$  nuclei and  $\text{V}^{3+}$  spins, and  $N_A$  is the Avogadro's number. The conventional way for calculating  $A_{\text{hf}}$  is to obtain it from the slope of a  $K$  versus  $\chi$  plot with  $T$  as an implicit parameter (figure 7), because  $\chi = (A_{\text{hf}}/(\mu_B \times N_A)) \times K$  is valid [26]. As can be seen in the inset of figure 7, the  $K$  versus  $\chi$  plot follows a linear behaviour at high temperatures ( $25 < T < 100\text{ K}$ ), yielding  $K_0 = 0.38(4)\%$  and  $A_{\text{hf}} = 4.72(1)\text{ kOe } \mu_B^{-1}$ .

## 4. Discussions

Centrosymmetric  $\text{La}_3[\text{WO}_6]_\infty[\text{VS}_{6/2}]$  remains paramagnetic down to, at least, 8 K according NMR data although anomalies are observed in specific heat and magnetic data at about 11 K. In an octahedron environment, two electrons have  $t_{2g}^2$  configuration and its product representation ( $t_2 \times t_2$ ) is reduced to  $^1A_1 + ^1E_1 + ^1T_2 + ^3T_1$  with  $^3T_1$  as the ground state [27], which is further split by a trigonal distortion into  $^3A + ^3E$  states [28]. The relative energies of these levels depend on whether the octahedra is distorted along the (1 1 1)-direction (3-fold rotation axis): either compressed in the title compound or elongated in  $\text{Ba}_3[\text{VSO}_3]_\infty[\text{VS}_{6/2}]$ . Both situations are schematically shown in figure 8. As  $\text{V}^{3+}$  in  $\text{Ba}_3[\text{VSO}_3]_\infty[\text{VS}_{6/2}]$  was not sitting at

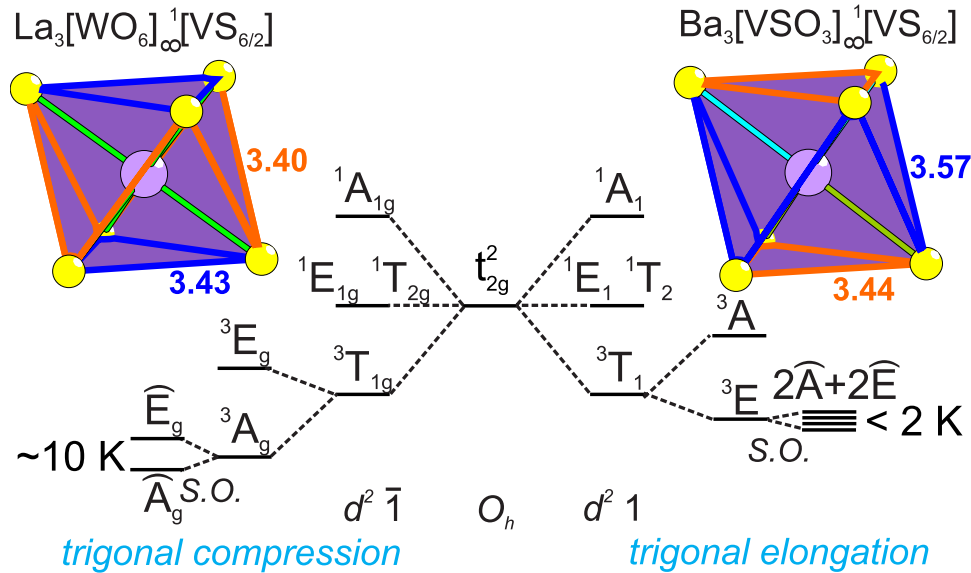


**Figure 8.** Proposed spin ground state of  $V^{3+}$  ( $3d^2$ ) in a perfect octahedron (center), in a  $VS_6$ -octahedron of  $La_3[WO_6]_\infty[VS_{6/2}]$  (left), and in a  $VS_6$ -octahedron of  $Ba_3[VSO_3]_\infty[VS_{6/2}]$  (right). The energy differences between levels are not correctly scaled.

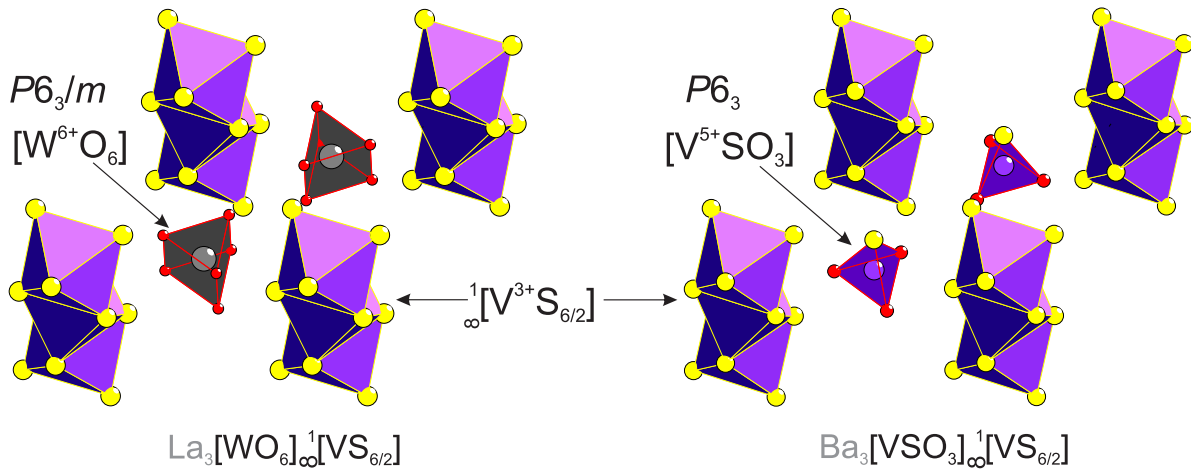


**Figure 9.** Arrangement of building units around V and W in the structures of  $La_3[WO_6]_\infty[VS_{6/2}]$  (left) and  $Ba_3[VSO_3]_\infty[VS_{6/2}]$  (right).

the coordination centre, the ‘g’ subscript was removed. In the title phase, the electron distribution ground state has three-fold degeneracy ( ${}^3A$ ), but when allowing for spin-orbit (S.O.) coupling the lowest excited state has no degeneracy ( $\widehat{A}$ ). Hence, a Schottky-like anomaly in the  $C_p(T)$  might agree with observations (figure 5).

When fitting a Schottky function, with doubly degenerated excited states, to the released entropy, there is an obvious discrepancy and the peak shape of the observed entropy release is less distinct, more symmetrical, and lacks the power-law like tail towards high temperatures. Yet, magnetic ordering phenomena are still not considered because that would contradict NMR data. However, by comparing with literature, a spin-orbital splitting was observed for a trigonally compressed octahedral coordination of  $V^{3+}$  in  $CsV(SO_4)_2 \cdot 12H_2O$  ( $4.93 \text{ cm}^{-1} \approx 7.1 \text{ K}$ ) [28], which would be similar to the suggested splitting for the title compound ( $\sim 10 \text{ K}$ , the maximum in  $\chi(T)$  in figure 4). In contrast, the ground state and the lowest excited states of Ba-compound is not well separated with

other states and a Schottky-like anomaly cannot be observed. Hence, only the local NMR probe, among the techniques presented here, was able to detect that the single ion anisotropy scenario is more probable than an ordering of spins.

It is worthwhile to compare the title compound with  $Ba_3[VSO_3]_\infty[VS_{6/2}]$  to emphasize similarities and differences as well as the unique situation of comparing almost identical magnetic chains (figure 9) with or without inversion symmetry. Both compounds are electronically highly correlated so the oxidation state of vanadium and its spin size should be the same. However,  $Ba_3[VSO_3]_\infty[VS_{6/2}]$  [23] lacks the crystallographic mirror plane perpendicular to the unique (c) axis and the space group in polar, non-centrosymmetric  $P6_3$  (No.173). The absence/presence of structural polarity is mainly caused by the structural unit residing between the magnetic chains: in the title compound, the trigonal prism  $WO_6$  can be described with a mirror plane perpendicular to the high-symmetry (3-fold rotation) axis of the unit and the magnetic chain is correspondingly highly symmetric. In contrast,



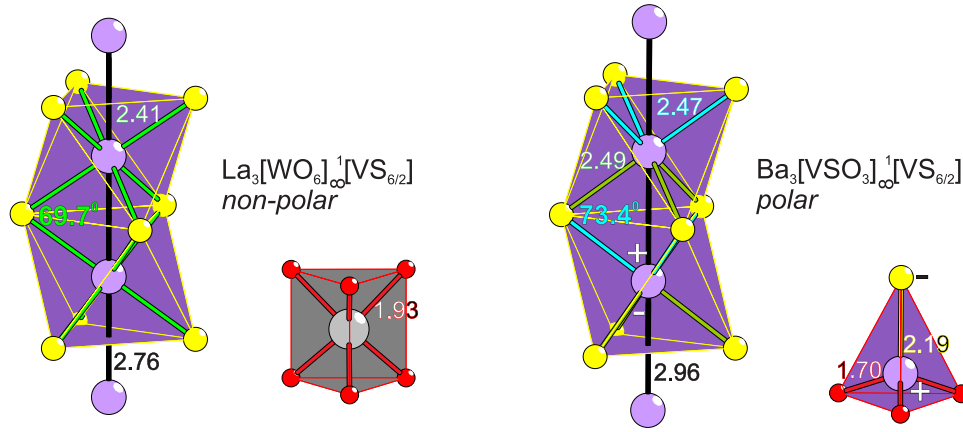


**Figure 10.** Parts of magnetic chains in  $\text{La}_3[\text{WO}_6]_{\infty}^1[\text{VS}_{6/2}]$  (left) and in  $\text{Ba}_3[\text{VSO}_3]_{\infty}^1[\text{VS}_{6/2}]$  (right) together with their corresponding non-polar  $[\text{WO}_6]$  and polar  $[\text{VSO}_3]$  structural motifs. Bond lengths are given in Å, the V–S–V bond angle in degrees, and the polarities are designated by pluses and minuses.

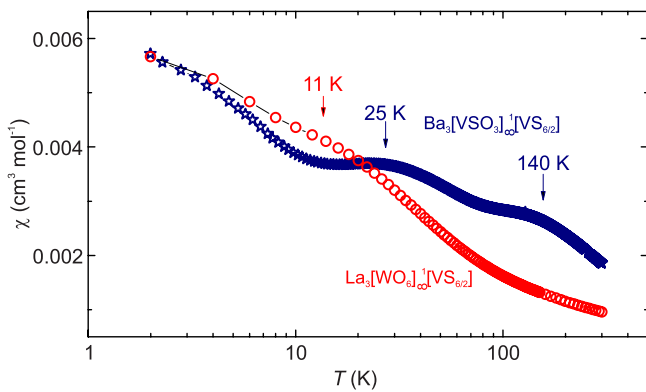


**Figure 11.** Comparison of magnetic susceptibilities of  $\text{La}_3[\text{WO}_6]_{\infty}^1[\text{VS}_{6/2}]$  (red) and  $\text{Ba}_3[\text{VSO}_3]_{\infty}^1[\text{VS}_{6/2}]$  (blue, data from [23]), as a function of temperature measured at  $\mu_0 H = 1$  T. Both curves were obtained on cooling in a magnetic field.

all  $\text{VSO}_3$  tetrahedra in  $\text{Ba}_3[\text{VSO}_3]_{\infty}^1[\text{VS}_{6/2}]$  are equally oriented and cause a global polarity. As a response,  $\text{V}^{3+}$  moves from the octahedral barycentre so that parts of this polarity are cancelled (figure 10) and two different V–S distances are observed.

With these minor differences in V-coordinations in mind, it is possible to compare these two compounds and their macroscopic properties, to extract information on the behaviour of an  $S = 1$  chain in the absence/presence of a crystallographic inversion centre ( $\bar{1}$ ). The here presented data for direct comparisons comprise magnetic susceptibility in the temperature range 300–2 K and magnetization at 2 K;  $\chi(T)$  data of  $\text{La}_3[\text{WO}_6]_{\infty}^1[\text{VS}_{6/2}]$  contain one anomaly at low temperatures close to 11 K (figure 11) is due to crystal field effects (see figure 8 with corresponding texts above).

Hence, the centrosymmetric compound is paramagnetic with strong antiferromagnetic spin–spin interactions at higher temperatures and, as low temperatures, single-ion anisotropy effects causes a deviation from simple paramagnetism. As an inversion symmetry is situated exactly between V site in the magnetic chain, at site 0,0,1/4 (Wyckoff 2a, site symmetry  $-6$ ),

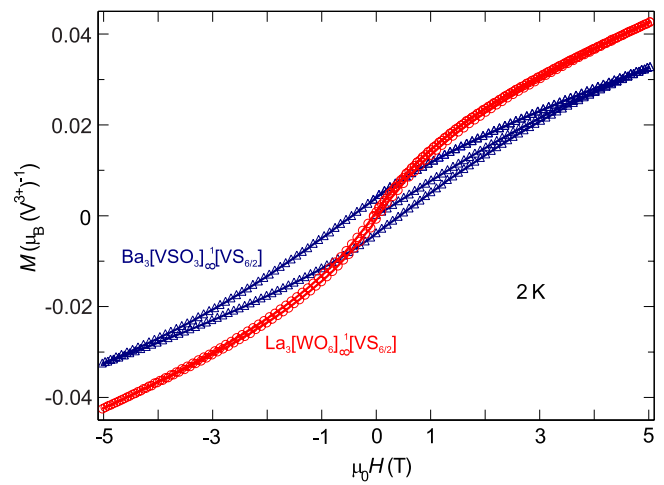


**Figure 12.** Comparison of magnetizations at 2 K for  $\text{La}_3[\text{WO}_6]_{\infty}^1[\text{VS}_{6/2}]$  (red) and  $\text{Ba}_3[\text{VSO}_3]_{\infty}^1[\text{VS}_{6/2}]$  (blue, data from [23]).

DMI in the title compound should be insignificant. Although strong anti-ferromagnetic spin–spin interactions also are obvious in  $\text{Ba}_3[\text{VSO}_3]_{\infty}^1[\text{VS}_{6/2}]$  ( $\theta_{\text{CW}} = -152$  K) [23] there are at least two, exceedingly broad, maxima in its  $\chi(T)$  data (at 25 and 140 K) that can neither be explained by local electron phenomena nor by long range magnetic orderings. Instead, the crystal symmetry probably plays a crucial role in understanding the high temperature  $\chi(T)$  maxima: these maxima then only appear if there is no inversion symmetry.

Because of intrinsic lattice electric polarity, higher order phenomena have to be considered and DMI [12, 13] are likely to be significant. DMI often prevent a collinear anti-ferromagnetic ground state; instead, the spins are canted out of the collinear state and a weak, residual ferromagnetic (non-compensated) component remains, which is possible to detect by magnetization measurements: in the field dependent magnetization data, the centrosymmetric title compounds only exhibit a minor saturating component on-top of a paramagnetic signal (figure 12), but the non-centrosymmetric

$\text{Ba}_3[\text{VSO}_3]_{\infty}^1[\text{VS}_{6/2}]$  exhibits a small but significant residual ferromagnetic signal, inferring that DMI might be active although no long range spin order has evolved.

A similar ferromagnetic component was observed in single crystals of non-centrosymmetric  $\text{YBaCo}_3\text{FeO}_7$  with quasi static spins as observed by Mössbauer spectroscopy but without long-range spin order as proven by neutron scattering experiments [29]. As  $\text{Ba}_3[\text{VSO}_3]_{\infty}^1[\text{VS}_{6/2}]$  most probably is a pyro-electric material, its weak temperature dependent electric polarity will be reflected in the very broad anomalies in the  $\chi(T)$  curve, as a result of DMI. However, this has to be further investigated at lower temperatures, on single crystal-line specimens, and/or with alternative techniques (like myon spin resonance) before these tentative postulations can be concluded on. Moreover, with magnetic and spectroscopic data from single crystals, it will be possible to estimate spin-to-spin interaction strengths ( $J_s$ ) and single ion anisotropies ( $D_s$ ). Subsequently, these novel  $S = 1$  magnetic chains can be compared with other similar magnetic systems, which exhibit systematics [1, 30].

The chemical flexibility of the here compared crystal structures [21–23] offer further possibilities for making detailed investigations as function of spin size in the presence of or lack of crystallographic inversion symmetry, which is a very rare, perhaps even unique, situation.

## 5. Conclusions

The crystal structure of novel, quasi-1D magnet  $\text{La}_3[\text{WO}_6]_{\infty}^1[\text{VS}_{6/2}]$  is described with a centrosymmetric space group. It is a strongly correlated electron system (insulator) where the chains of almost octahedrally coordinated  $\text{V}^{3+}$  ions carry well-defined  $S = 1$  moments and the spin–spin interactions are strong and anti-ferromagnetic but without magnetic long range order above 2 K. Observed crystal fields suggest single ion anisotropy, which also agree with observation by NMR spectroscopy, magnetic data at low temperatures, and a Schottky-like anomaly in the specific heat data. By detailed comparison with non-centrosymmetric compound  $\text{Ba}_3[\text{VSO}_3]_{\infty}^1[\text{VS}_{6/2}]$  with a similar magnetic lattice, it is possible to conclude that the crystallographic inversion symmetry has a large influence on the behaviour of the magnetic chains; for the lattice without inversion symmetry magnetoelectric coupling is evident through extra anomalies in the magnetic susceptibility data. These crystal structures constitute model systems for 1D magnetic chains with the spin-size and the presence or absence of inversion symmetry as free parameters.

## Acknowledgments

This work was funded by the German Science Foundation (DFG) through project VA 831/4-1. We are grateful for Andrew Fitch's help during the measurements at ID22 (ESRF,

Grenoble, France). The research of JKK was supported by the Max Planck-POSTECH Center for Complex Phase Materials. We also thank Chun-Fu Chang for organizing JKK's student exchange program.

## ORCID iDs

K M Ranjith  <https://orcid.org/0000-0001-8681-2461>

M Valldor  <https://orcid.org/0000-0001-7061-3492>

## References

- [1] Wierschem K and Sengupta P 2014 *Mod. Phys. Lett. B* **28** 1430017
- [2] Gambardella P, Dallmeyer A, Maiti K, Malagoli M C, Eberhardt W, Kern K and Carbone C 2002 *Nature* **416** 301
- [3] Segovia P, Purdie D, Hengsberger M and Baer Y 1999 *Nature* **402** 504
- [4] Blumenstein C, Schäfer J, Mietke S, Meyer S, Dollinger A, Lochner M, Cui X Y, Patthey L, Matzdorf R and Claessen R 2011 *Nat. Phys.* **7** 776
- [5] Haldane F D M 1980 *Phys. Rev. Lett.* **45** 1358
- [6] Haldane F D M 1981 *J. Phys. C: Solid State Phys.* **14** 2585
- [7] Affleck I 1989 *J. Phys.: Condens. Matter* **1** 3047
- [8] Affleck I 1990 *Phys. Rev. B* **41** 6697
- [9] Fiebig M, Lottermoser T, Meier D and Trassin M 2016 *Nat. Rev. Mater.* **1** 16046
- [10] Tokura Y, Seki S and Nagaosa N 2014 *Rep. Prog. Phys.* **77** 076501
- [11] Hou Z *et al* 2017 *Adv. Mater.* **29** 1701144
- [12] Dzyaloshinsky I 1958 *J. Phys. Chem. Solids* **4** 241
- [13] Moriya T 1960 *Phys. Rev.* **120** 91
- [14] Zheludev A, Maslov S, Shirane G, Sasago Y, Koide N and Uchinokura K 1997 *Phys. Rev. Lett.* **78** 4857
- [15] Urcelay-Olabarria I *et al* 2017 *Phys. Rev. B* **96** 104435
- [16] Yasui Y, Yanagisawa Y, Okazaki R and Terasaki I 2013 *Phys. Rev. B* **87** 054411
- [17] Lorenz T 1999 *Adv. Solid State Phys.* **39** 301
- [18] Hase M, Terasaki I and Uchinokura K 1993 *Phys. Rev. Lett.* **70** 3651
- [19] Seidel A, Marianetti C A, Chou F C, Ceder G and Lee P A 2003 *Phys. Rev. B* **67** 020405
- [20] Bryhan D N, Rakers R, Klimaszewski K, Patel N, Bohac J J, Kremer R K, Mattausch H and Zheng C 2010 *Z. Anorg. Allg. Chem.* **636** 74
- [21] Kim J K, Lai K T and Valldor M 2017 *J. Magn. Magn. Mater.* **435** 126
- [22] Calvagna F, Zhang J-H, Li S-J and Zheng C 2001 *Chem. Mater.* **13** 304
- [23] Hopkins E J *et al* 2015 *Chem. Eur. J.* **21** 7938
- [24] Schutte W J, de Boer J L and Jellinek F 1987 *J. Solid State Chem.* **70** 207
- [25] Bain G A and Berry J F 2008 *J. Chem. Educ.* **85** 532
- [26] Nath R, Ranjith K M, Roy B, Johnston D C, Furukawa Y and Tsirlin A A 2014 *Phys. Rev. B* **90** 024431
- [27] Sugano S 1970 *Multiplets of Transition-Metal Ions in Crystals* (New York: Academic)
- [28] Best S P and Clark R J H 1985 *Chem. Phys. Lett.* **122** 401
- [29] Valldor M, Hermann R P, Wuttke J, Zamponi M and Schweika W 2011 *Phys. Rev. B* **84** 224426
- [30] Sakai T and Takahashi M 1990 *Phys. Rev. B* **42** 4537